Supporting Information

Laboratory investigation of renoxification from the photolysis of inorganic particulate nitrate

Qianwen Shi[1], Ye Tao[1], Jordan E. Krechmer[2], Colette L. Heald[3], Jennifer G. Murphy[4], Jesse H. Kroll[3] and Qing Ye[3*]

1. Department of Physical and Environmental Sciences, University of Toronto Scarborough, Toronto, Ontario M1C 1A4, Canada
2. Center for Aerosol and Cloud Chemistry, Aerodyne Research Incorporated, Billerica, Massachusetts 01821, United States
3. Department of Civil and Environmental Engineering, Massachusetts Institute of Technology, Cambridge, Massachusetts 02139, United States
4. Department of Chemistry, University of Toronto, Toronto, Ontario M5S 3H6, Canada

* Corresponding author, qye@mit.edu, 77 Massachusetts Avenue, Massachusetts Institute of Technology, 48-330, Cambridge, MA 02139, USA

1. Determination of measured j_{NO_2}

NO_2 was injected from a gas cylinder (Airgas) into the chamber filled with the ultra-zero gas (Airgas) to generate a typical mixing ratio of 50 ppb. Then, all 18 lights were switched on to initiate NO_2 photolysis. After several minutes for equilibration, concentrations of NO, NO_2 and O_3 were measured to derive $j_{NO_{2,actinometry}}$ assuming steady state:

$$j_{NO_{2,actinometry}} = \frac{k_{O_3+NO}\,[NO][O_3]}{[NO_2]}$$

where $k_{O_3+NO} = 1.8 \times 10^{-14}$ cm^3 $molec^{-1}$ s^{-1}. The j_{NO_2} measurement was performed every month to monitor the conditions of the lights. Over the course of 5 months, there was <15% variation in $j_{NO_{2,actinometry}}$ with an average value of 0.46 min^{-1} under UVA condition and 0.23 min^{-1} under UVB condition.

2. Instruments:

2.1 Interference in the NO_{xy} analyzer:

The blue-light converter (BLC) could have potential interferences from the photolysis products of VOCs reacting with NO[1] and the thermal decomposition of NO_y[2,3] within the photolysis cell. Under our experimental conditions, these interferences were negligible. Limits of detection were determined by passing ultra-zero air to the instrument for a continuous period and calculating the Allan Variance of the signals (**Figure S3**). Channel 2 is also able to measure total reactive nitrogen (NO_y) by adding a molybdenum catalytic converter (Mo) that operated at 300 °C. The NO_y channel was not used in the experiments but was used for HNO_3 and HONO calibration in the I-CIMS.

2.2 Time-of-flight iodide chemical ionization mass spectrometry

Measurements of HONO and HNO_3 by the I-CIMS were calibrated by the NO_y channel in the NO_{xy} analyzer. During calibrations, gaseous HONO or HNO_3 was generated by flowing ultra-zero gas above an aqueous HONO or HNO_3 solution. The HONO solution was prepared by mixing dilute $NaNO_2$ solution and H_2SO_4 solution. Channel 1 and channel 2 of the NO_{xy}

analyzer are used to measure NO_x and total NO_y respectively in the calibration. The mixing ratios of HONO and HNO_3 are calculated as [HONO] or $[HNO_3] = [NO_y] - [NO_x]$, and therefore side products like NO_2 emitted from HONO sources are subtracted from the NO_y concentration. The effective sensitivities of I-CIMS were determined to be 1.85 counts ppt^{-1} and 11.38 counts ppt^{-1} for HONO and HNO_3, respectively. The loss of HONO in the sampling lines was small while HNO_3 had considerable line loss. Therefore, the HNO_3 sensitivity represented an upper-bound estimate. The time-of-flight extraction frequency for the calibration measurements was 20 kHz.

2.3 Denuder collections and Ion chromatography (IC)

Multi-channel 242-mm-long annular denuders (URG, Corp. USA) were used for sampling of gaseous nitrous acid and nitric acid. Denuders were coated with 1% Na_2CO_3 and 1% glycerol in methanol: H_2O = 1:1 solution. The denuders were dried with a mild flow of high-purity N_2 (~ 2 cm^3 min^{-1}). The extraction of denuder was performed with 10 ml DI water followed by the immediate measurement on the IC (Thermo Fisher). The interference from the background of N_2 drying gas was assessed by passing through a short three-channel 100-mm-long denuder (coated with the same coating solution and dried) prior to passing through the denuder that was being prepared. No interferences from the drying gas were found. Under the low sampling flow (~1 cm^3 min^{-1}) used in this study, near-complete sampling efficiencies of acidic gaseous components should be valid. The reactivity of carbonate-coated surface to NO_2 is very low, with the efficiency ranging from 0.5 to 2% [4]. The detection limits in the IC are 2.9 ng mL^{-1} for nitrate and 3.2 ng mL^{-1} for nitrite, corresponding to an average mixing ratio of 1.64 ppb and 0.95 ppb, for HNO_3 and HONO respectively, in a typical experiment with 20 minutes of flow through the denuder. However, because of highly variable signals in the denuder blanks, the detection limits for denuder samples (3σ) are 50 ng mL^{-1} for nitrate and 5.4 ng mL^{-1} for nitrite, corresponding to an average mixing ratio of 28.3 ppb and 1.60 ppb.

2.4 Aerosol mass spectrometer and scanning particle mobility sizer

An aerosol mass spectrometer (AMS) and a scanning particle mobility sizer (SMPS) were used to monitor the concentration of particulate nitrate in the chamber. The transmission efficiency for particles between 70 – 700 nm in the AMS inlet is close to unity. This size range

covered the majority (>95%) of the particle mass generated by the atomizer. The ionization efficiency of the AMS was calibrated using ammonium nitrate particles. The SMPS size measurements were calibrated using monodisperse polystyrene latex spheres. The size range of the SMPS was 15 – 660 nm.

3. Determination of particulate nitrate concentration in the chamber

The determination of $j_{\mathrm{pNO_3^-}}$ (the photolysis rate constant for particulate nitrate) requires the calculation of $\mathrm{pNO_3^-}_{\ \mathrm{total}}$ (total nitrate particles inside the chamber), $\mathrm{pNO_3^-}_{\ \mathrm{suspended}}$ (nitrate particles in suspension inside the chamber) and $\mathrm{pNO_3^-}_{\ \mathrm{wall}}$ (nitrate particles that have lost to the chamber wall). Since the chemical loss of nitrate due to photolysis is negligible compared to compared particle wall loss and dilution loss, the change in the concentration of $\mathrm{pNO_3^-}_{\ \mathrm{suspended}}$ is determined by wall loss and dilution loss:

$\frac{d\mathrm{pNO_3^-}_{\mathrm{suspended}}}{dt} = -k_{sum} * \mathrm{pNO_3^-}_{\mathrm{suspended}}$ and $k_{sum} = k_{dil} + k_{wall}$,

where k_{dil} and k_{wall} are the first-order rate constants for mass loss due to chamber dilution and deposition onto the chamber wall, respectively. $\mathrm{pNO_3^-}_{\mathrm{suspended}}$ was measured by the SMPS, and an exponential decay was fitted to get k_{sum}. k_{dil} is known given the dilution flow of the chamber and the total volume of the chamber assuming that the dilution of the suspended particles is the same as the dilution of the gas flow. Therefore, k_{wall} is known by subtracting k_{dil} from k_{sum}. The average k_{wall} was 0.09 ± 0.03 min^{-1} in the experiments. k_{wall} is then used to calculate $\mathrm{pNO_3^-}_{\ \mathrm{wall}}$ by solving $\frac{d\mathrm{pNO_3^-}_{\mathrm{wall}}}{dt} = k_{wall} * \mathrm{pNO_3^-}_{\mathrm{suspended}}$ assuming particles lost onto the wall would not get diluted out of the chamber. Lastly, $\mathrm{pNO_3^-}_{\ \mathrm{total}} = \mathrm{pNO_3^-}_{\ \mathrm{suspended}} + \mathrm{pNO_3^-}_{\ \mathrm{wall}}$.

4. In-particle nitrite ion concentration

Ion chromatography was used during some of the experiments to measure the ensemble [NO_2^-] and [NO_3^-] in particles that were collected on filters. We compare the [NO_2^-] : [NO_3^-] in experiments that yielded different photolysis rate constants and in the blank experiments (no lights were turned on). The results are shown below:

$j_{pNO_3^-}$ (s^{-1})	$[NO_2^-] : [NO_3^-]$
0 (dark)	0.015
0 (dark)	0.054
9.70E-07	0.027
3.64E-06	0.054
8.27E-06	0.034
2.19E-05	0.041

The presence of the small amount of NO_2^- in the dark samples may come from impurities in the $NaNO_3$ solution. When comparing the ratios to those from experiments with different aerosol nitrate photolysis rate constants (shown in the table), we do not see any systematic increase. In addition, the majority of nitrite produced within the particle from nitrate photolysis would be expected to photolyze (or evaporate as HONO) itself. The fact that nitrite/nitrate remains low, and is independent of light levels in the chamber, implies that nitrite is not accumulating in the particles.

5. Box model:

The model conditions are the following:

Temperature: 298 K.

Relative humidity: 70% for UVA and 85% for UVB (highest RH conditions accessed in the experiments, corresponding to the fastest measured renoxification rates). The humidified dilution flow, which was generated via passing dry zero air through a bubbler filled with DI water, was higher in UVA experiments than UVB experiments due to the flow requirements of the I-CIMS used in UVA experiments. Therefore, the lower RH in UVA experiments was due to the less efficient humidification in the bubbler for the larger dilution flow in UVA conditions.

Background concentration: NO_2 = 0.4 ppb, NO = 0.05 ppb, HONO = 0.04 ppb, HNO_3 = 0.09 ppb (typical background concentration of the chamber).

Time: 1200 s (typical experiment time for photolysis on particles).

Total renoxification rate constant: 20×10^{-6} under UVB and 3×10^{-6} under UVA. These numbers are derived from the measurements under the highest RH conditions when NO_x, HONO and HNO_3 measurements were all available.

A full list of reactions can be found in Framework for 0-D Atmospheric Modeling (F0AM). Simulation results are presented in **Figure S9**. Below are the reactions that involve nitrogen-containing species:

$O + NO \rightarrow NO_2$

$O + NO_2 \rightarrow NO$

$O + NO_2 \rightarrow NO_3$

$NO + O_3 \rightarrow NO_2$

$NO_2 + O_3 \rightarrow NO_3$

$NO + NO \rightarrow NO_2 + NO_2$

$NO + NO_3 \rightarrow NO_2 + NO_2$

$NO_2 + NO_3 \rightarrow NO + NO_2$

$NO_2 + NO_3 \rightarrow N_2O_5$

$OH + NO \rightarrow HONO$

$OH + NO_2 \rightarrow HNO_3$

$OH + NO_3 \rightarrow HO_2 + NO_2$

$HO_2 + NO \rightarrow OH + NO_2$

$HO_2 + NO_2 \rightarrow HO_2NO_2$

$OH + HO_2NO_2 \rightarrow NO_2$

$HO_2 + NO_2 \rightarrow OH + NO_2$

$OH + HONO \rightarrow NO_2$

$OH + HNO_3 \rightarrow NO_3$

$HNO_3 \rightarrow NA$

$N_2O_5 \rightarrow NA + NA$

$NO_2 + h\nu \rightarrow NO + O$

$NO_3 + h\nu \rightarrow NO$

$NO_3 + h\nu \rightarrow NO_2 + O$

$HONO + h\nu \rightarrow OH + NO$

$HNO_3 + h\nu \rightarrow OH + NO_2$

$N_2O_5 \rightarrow NO_2 + NO_3$

$HO_2NO_2 \rightarrow HO_2 + NO_2$

$pNO_3^- + h\nu \rightarrow NO_2$

pNO_3^- + hν → HONO

pNO_3^- + hν → NO

6. Particle pH estimation

The pH of ammonium nitrate (NH_4NO_3) particles was estimated using the Model III of Extended Aerosol Inorganics Model, E-AIM.[5–7] The temperature is fixed at 298.15 K for Model III and the inputs we used include the relative humidity (0.5 and 0.7), inorganic compositions of Na^+, NH_4^+, NO_3^-, SO_4^{2-} and NH_3 in moles m^{-3}. The upper limit of NH_3 for E-AIM calculation was around 10 ppm therefore we ran the model with 1 to 10 ppm of NH_3 and then extrapolated the pH of NH_4NO_3 particle to 50-100 ppm of NH_3 (Figure S8). In general, the estimated pH of NH_4NO_3 particles under our experiment conditions ranged between 6.2 to 6.6.

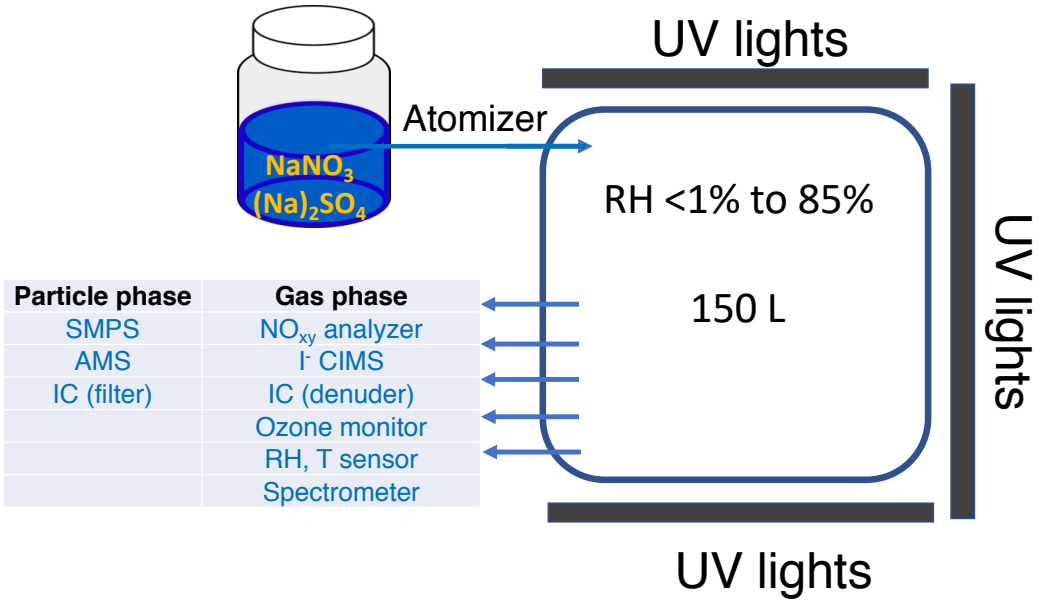

Figure S1: Experimental setup for laboratory photolysis experiments of particulate sodium and ammonium nitrate. The 150 L reaction chamber was surrounded by 18 UV lights. Particulate nitrate was generated via atomizing 10 g L^{-1} $NaNO_3$ (or NH_4NO_3, or $NaNO_3$ with added photosensitizers) and 2 g/L $(Na)_2SO_4$ solution. Multiple analytical instruments were used to measure the concentration of particle- and gas-phase nitrogen-containing species. In addition, a total backup flow of ~ 8 lpm was continuously injected into the chamber to balance the sample flow pulled by the instruments.

Table S1: A list of instruments used in this study and their uncertainties and limits of detection (LOD).

Instrument	Measurement	Uncertainty	LOD
SMPS	Particle size and volume	< 2% in DMA	2.5 nm for CPC
AMS	Particle composition	± 38 %[8]	2.9 ng m^3
NO_{xy} analyzer	NO	± 6%	41 ppt s^{-1}
	NO_2	± 12%	52 ppt s^{-1}
	NO_x	± 10%	68 ppt s^{-1}
	NO_y	± 10%	48 ppt s^{-1}
I^- CIMS	HONO, HNO_3		7.3 ppt in 15 s[9]
IC (denuder)	HONO		1.63 ppb
	HNO_3		28.3 ppb
Ozone monitor	O_3	1.5 ppb	3 ppb in 10 s
	RH, Temperature	± 2 % at 50%	
Spectrometer	Photon flux	1.5 nm FWHM	

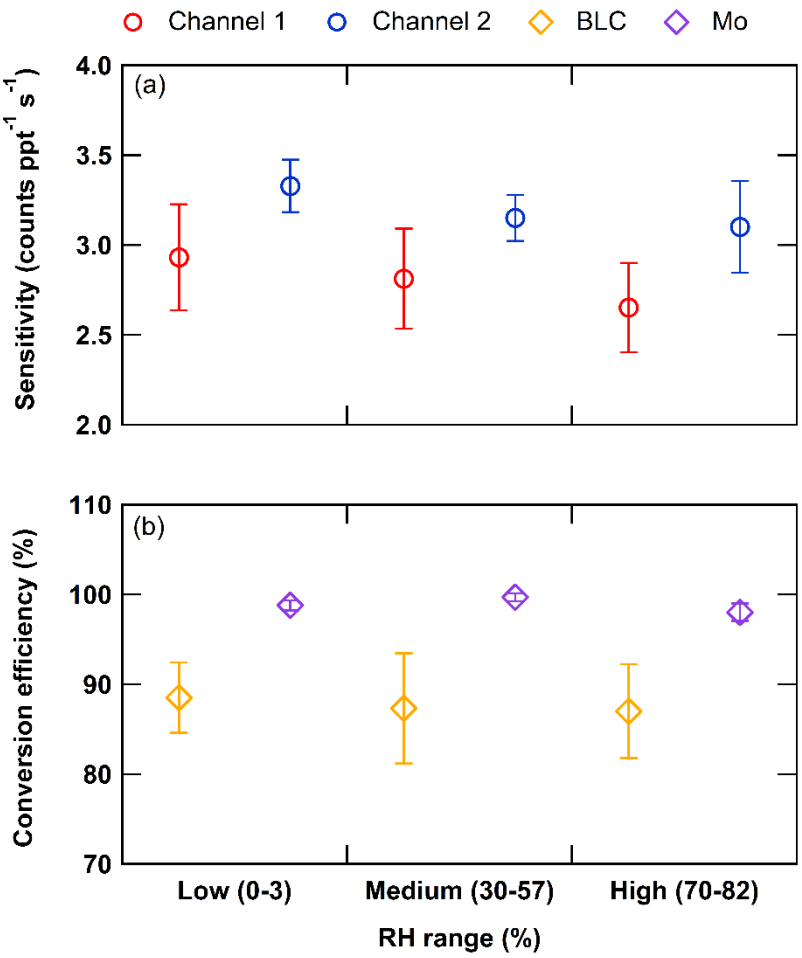

Figure S2: Sensitivity of NO_{xy} analyzer at different RH ranges for channel 1 and 2, blue-light converter (BLC) and Mo converter conversion efficiency. The slight decrease in instrument sensitivity at higher RH may be due to quenching, while the converter's efficiency is little affected by RH.

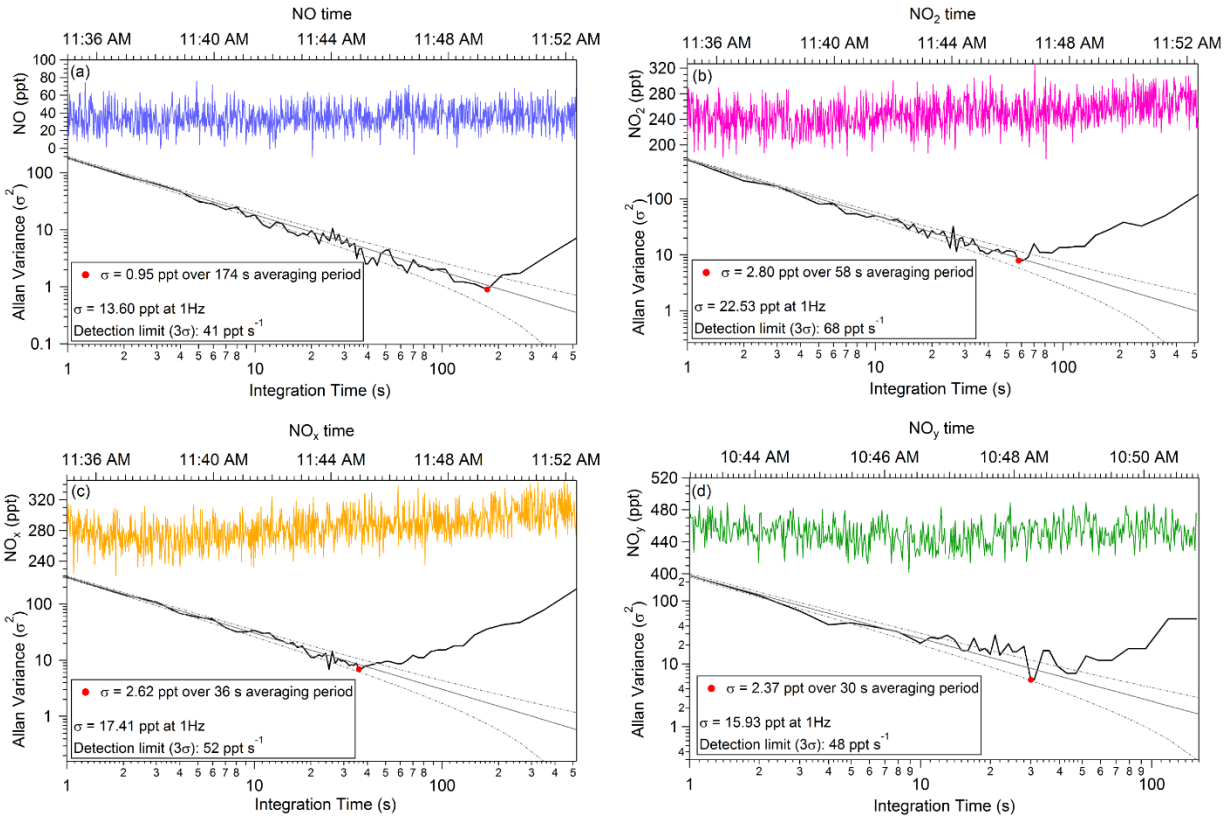

Figure S3: Allan variance plots of NO, NO_2, NO_x and NO_y measured by the NO_{xy} analyzer. In each subplot, upper traces represent the 1Hz data collected; lower traces show the Allan variance of the corresponding data. Detection limit was calculated as 3σ at 1 second integration time.

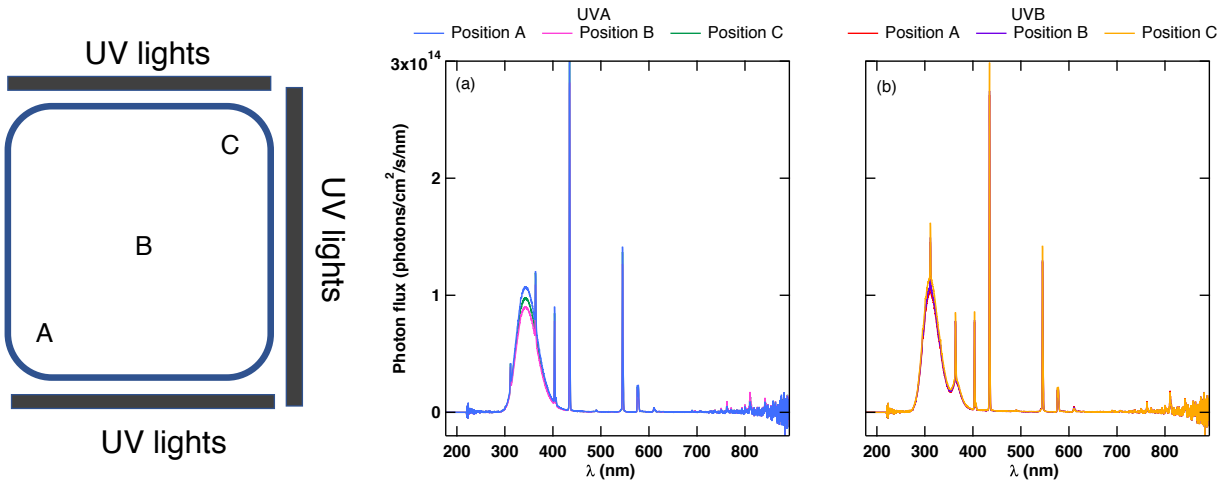

Figure S4: Heterogeneity of photon flux in different locations inside the chamber measured by the spectrometer. The effective photon flux in the center of the chamber (position B), which is scaled using the photolysis rate of NO_2 is shown in Figure 2. For both types of UV lights, there is minimal heterogeneity of photon flux inside the chamber. Therefore, we assume that all particles in the chamber are exposed to the same level of irradiation within each experiment.

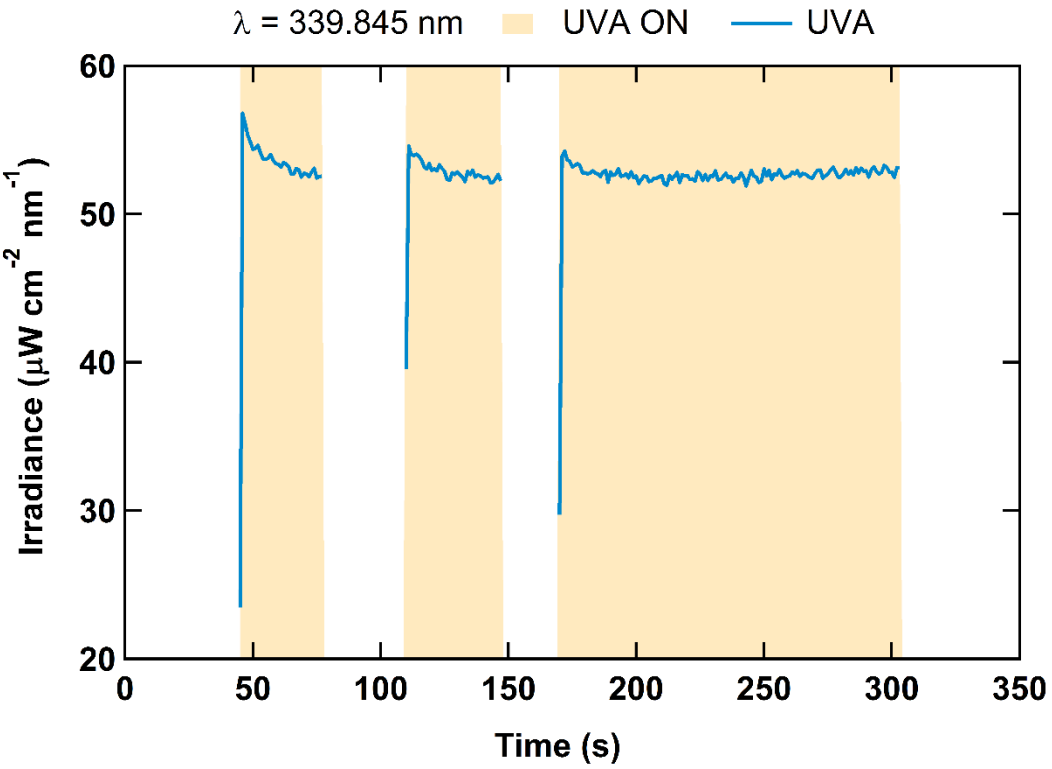

Figure S5: Irradiance of UVA lamps at 340 nm (the peak of the irradiance measured by the spectrometer) during three quick on-off cycles. Despite a short and small burst of photons after the first couple seconds, the irradiance stays relatively constant. Therefore, we assume constant light conditions over the course of each experiment.

Table S2: A summary of all experiments conducted, showing the particulate nitrate investigated, light (UVA/UVB) and RH conditions, results as enhancement factor (Figure 3) or NO_x production rate constant (Figure 4), and the corresponding figures.

Particle types[a]	Light	RH (%)	Enhancement factor	NO_x production rate constant (s^{-1})	Figure
$NaNO_3$	UVA	35	0.47 ± 0.03	-	3
		36	0.12 ± 0.07	-	3
		50	0.78 ± 0.12	-	3
		66	0.67 ± 0.05	1.85E-6 ± 1.28E-7	3,4
		70	1.20 ± 0.19	-	3
$NaNO_3$, wall loss	UVA	50	0.73 ± 0.02		S7
$NaNO_3$	UVB	3	0.00 ± 0.00	-	3
		32	0.12 ± 0.01	-	3
		35	0.05 ± 0.01	-	3
		43	0.38 ± 0.03	-	3
		56	1.47 ± 0.41	2.98E-6 ± 2.40E-7	3,4
		74	0.76 ± 0.08	-	3
		80	0.44 ± 0.28	-	3
		85	1.09 ± 0.67	-	3
$NaNO_3$, wall loss	UVB	36	0.14 ± 0.09		S7
		80	0.23 ± 0.01		S7
$NaNO_3$	UVB	70	-	3.04E-6 ± 6.18E-7	4
$NaNO_3$ + IM-CHO 0.013 g/L		75	-	4.54E-6 ± 3.93E-7	4
$NaNO_3$ + IM-CHO 0.039 g/L		70	-	4.48E-6 ± 5.71E-7	4
$NaNO_3$ + IM 2.3 g/L		71	-	5.30E-6 ± 8.47E-7	4
$NaNO_3$ + IM 2.3 g/L		76	-	2.69E-6 ± 3.57E-7	4
$NaNO_3$ + PA 0.013 g/L		70	-	2.03E-6 ± 2.97E-7	4
NH_4NO_3	UVA	70	-	5.33E-6 ± 4.58E-7	4
	UVB	50	-	6.25E-6 ± 1.01E-6	4
		70	-	8.23E-6 ± 7.06E-7	4

a: 2 g L^{-1} sodium sulfate was added in all solutions that were used to generate the particles.

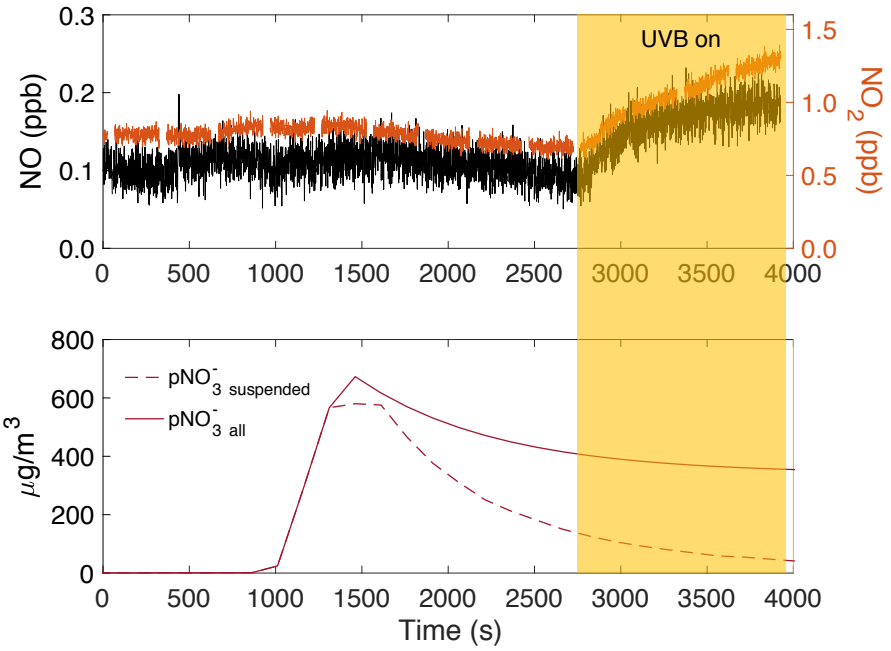

Figure S6: Time series of NO, NO_2 and nitrate particle concentration in a "wall loss" experiment. Lights were turned on after the majority of the suspended particles lost to the wall.

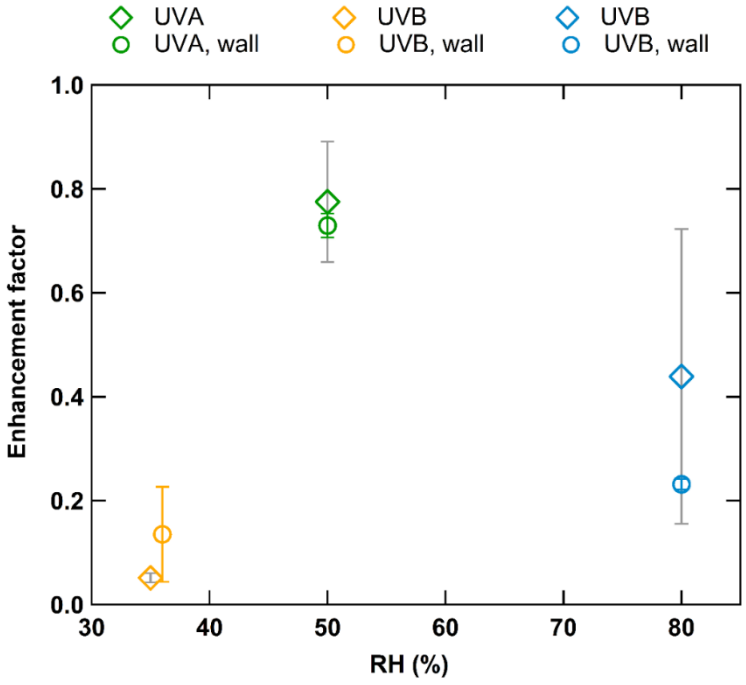

Figure S7: Enhancement factors from standard experiments (diamonds) described in the main text and those from experiments in which we photolyzed the particles after the majority of the particles were lost to the chamber wall (circles) under a range of RH.

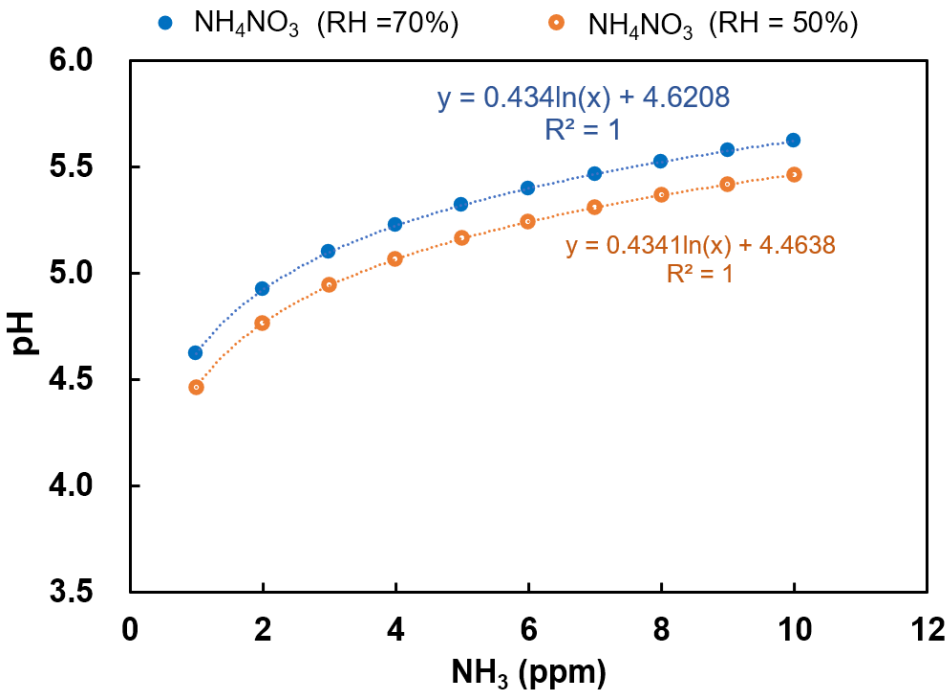

Figure S8: E-AIM estimations of pH change of NH_4NO_3 particles with respect to gas-phase NH_3 mixing ratio present in the system under 50% and 70% RH. By extrapolation, the pH range for NH_4NO_3 particles when NH_3(g) level is 50 – 100 ppm is 6.2 - 6.5 (50% RH) and 6.3 -6.6 (70%).

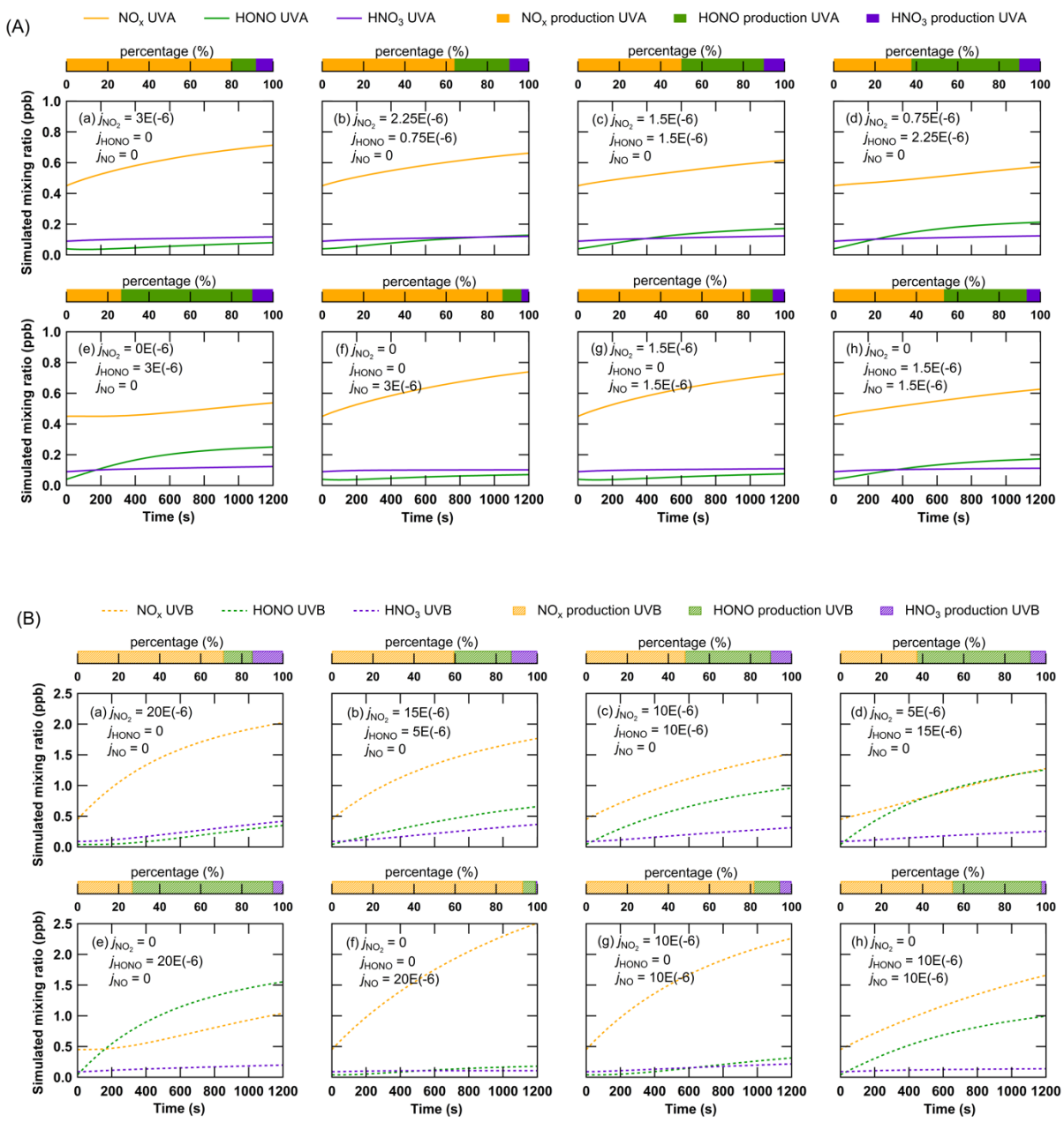

Figure S9: F0AM model simulations under UVA (panel A) at 70% RH and UVB (panel B) at 85% RH. The simulations were performed assuming different product molar ratios of NO_2, HONO, and NO with a constant particulate nitrate concentration of 150 ppb. J (in s^{-1}) is the production rate constants. On top of each plot, the fractional contributions of NO_x, HONO, and HNO_3 at the end of the experiments from the simulations are shown. We combined the simulated fraction of HONO and HNO_3 and the measured NO_x to derive range of total photolysis rate constant for experiments when HONO and HNO_3 measurements

were not available. This helps us to estimate the possible range of enhancement factor with respect to HNO_3 photolysis.

Reference

(1) Villena, G.; Bejan, I.; Kurtenbach, R.; Wiesen, P.; Kleffmann, J., Interferences of Commercial NO_2 Instruments in the Urban Atmosphere and in a Smog Chamber. *Atmos. Meas. Tech.* **2012**, *5* (1), 149–159. https://doi.org/10.5194/amt-5-149-2012.

(2) Reed, C.; Evans, M. J.; Di Carlo, P.; Lee, J. D.; Carpenter, L. J., Interferences in Photolytic NO_2 Measurements: Explanation for an Apparent Missing Oxidant? *Atmos. Chem. Phys.* **2016**, *16* (7), 4707–4724. https://doi.org/10.5194/acp-16-4707-2016.

(3) McClenny, W. A.; Williams, E. J.; Cohen, R. C.; Stutz, J., Preparing to Measure the Effects of the NO_x SIP Call - Methods for Ambient Air Monitoring of NO, NO_2, NO_y, and Individual NO_z Species. *J. Air Waste Manag. Assoc.* **2002**, *52* (5), 542–562. https://doi.org/10.1080/10473289.2002.10470801.

(4) Allegrini, I.; De Santis, F.; Di Palo, V.; Febo, A.; Perrino, C.; Possanzini, M.; Liberti, A., Annular Denuder Method for Sampling Reactive Gases and Aerosols in the Atmosphere. *Sci. Total Environ.* **1987**, *67* (1), 1–16. https://doi.org/10.1016/0048-9697(87)90062-3.

(5) Wexler, A. S.; Clegg, S. L., Atmospheric Aerosol Models for Systems Including the Ions H^+, NH_4^+, Na^+, SO_4^{2-}, NO_3^-, Cl^-, Br^-, and H_2O. *J. Geophys. Res.* **2002**, *107*, 14-1-14–14. https://doi.org/110.1029/2001JD000451.

(6) Clegg, S. L.; Brimblecombe, P.; Wexler, A. S., Thermodynamic Model of the System H^+–NH_4^+–Na^+–SO_4^{2-}–NO_3^-–Cl^-–H_2O at 298.15 K . *J. Phys. Chem. A* **1998**, *102* (12), 2155–2171. https://doi.org/10.1021/jp973043j.

(7) Clegg, S. L.; Pitzer, K. S.; Brimblecombe, P., Thermodynamics of Multicomponent, Miscible, Ionic Solutions. 2. Mixtures Including Unsymmetrical Electrolytes. *J. Phys. Chem.* **1992**, *96* (23), 9470–9479. https://doi.org/10.1021/j100202a074.

(8) Jimenez, J. L.; Canagaratna M. R.; Drewnick, F. D.; Allan, J. D.; Alfarra, M. R.; Middlebrook, A. M.; Slowik, J. G.; Zhang, Q.; Coe, H.; Jayne, J. T.; Douglas, R. W., Comment on "The effects of molecular weight and thermal decomposition on the sensitivity of a thermal desorption aerosol mass spectrometer"." *Aerosol Sci. Tech,* **2016**, 50 (9): i–xv.

(9) Lee, B. H.; Lopes-Hilfiker, F. D.; Mohr, C.; Kurtén, T.; Worsnop, D. R.; Thornton, J. A., An iodide-adduct high-resolution time-of-flight chemical-ionization mass spectrometer: Application to atmospheric inorganic and organic compounds." *Environ. Sci. Tech.* **2014***,* 48 (11), 6309–6317.